

## Comparative Seismic Assessment of Steel Moment-Resisting Frames Using Real and Artificial Spectrum-Matched Records under Multiple Soil Conditions

Cigdem Avci Karatas<sup>1\*</sup>, Kivanc Taskin<sup>2</sup>, Kerem Peker<sup>3</sup>, Mustafa Kulak<sup>2</sup>

<sup>1</sup>Yalova University, Faculty of Engineering, Department of Transportation Engineering, Yalova, Türkiye, [cigdem.karatas@yalova.edu.tr](mailto:cigdem.karatas@yalova.edu.tr), [ror.org/01x18ax09](http://ror.org/01x18ax09)

<sup>2</sup>Eskisehir Technical University, Faculty of Engineering, Department of Civil Engineering, Eskisehir, Türkiye, [kivanct@eskisehir.edu.tr](mailto:kivanct@eskisehir.edu.tr), [mkulak@windowslive.com](mailto:mkulak@windowslive.com), [ror.org/00gcgv39](http://ror.org/00gcgv39)

<sup>3</sup>Erdemli Engineering and Consulting Co. Ltd., Istanbul, Türkiye, [peker@erdemli.com](mailto:peker@erdemli.com)

\*Corresponding Author

### ARTICLE INFO

### ABSTRACT

Keywords:  
Steel MRFs  
Seismic performance  
Spectrum matching  
Time-history analysis  
Soil classification



#### Article History:

Received: 14.07.2025

Revised: 08.09.2025

Accepted: 26.11.2025

Online Available: 28.01.2026

This study investigates the seismic response of steel moment-resisting frames (MRFs) using linear time-history analysis (LTHA) to evaluate the influence of real and artificial spectrum-matched ground-motion records under multiple soil conditions. Three archetype buildings—3-, 9-, and 20-story—were modeled according to the SAC Steel Project (FEMA 355-C Appendix B) and analyzed using SAP2000® to assess their comparative performance under different spectral inputs. The analysis employed three types of seismic spectra: The Elastic Spectrum (ES), Reduced Turkish Earthquake Code (TEC-2018) Spectrum, and Reduced ASCE Spectrum across four local soil classes (ZA–ZD). A total of 252 earthquake ground motions, including real and artificial records, were used. The results revealed that artificial records achieved smoother spectral compatibility and more stable base shear predictions, whereas real records induced higher variability owing to their natural frequency content and phase characteristics. This divergence was most significant in softer soils (ZC and ZD), with base shear variations of up to  $\pm 35\%$ . The findings highlight the need to integrate both record types into seismic assessments and contribute to the advancement of performance-based earthquake engineering approaches.

## 1. Introduction

Inadequate building safety remains a major concern, often leading to significant structural damage and casualties during earthquakes [1]. Türkiye, situated in a seismically active region, has undergone substantial advancements in building design, structural analysis, and seismic regulations, particularly after the 1999 Izmit/Kocaeli/Gölcük (Mw 7.4) and Düzce (Mw 7.1) earthquakes. These catastrophic events underscore the necessity for stricter seismic design standards and the adoption of more sophisticated engineering methodologies to improve earthquake resilience [1].

The Turkish Earthquake Code (TEC-2007) [2] was implemented in 2007 to establish seismic design specifications for buildings in earthquake-prone regions. However, challenges in interpreting and applying the TEC-2007 highlight the need for regulatory revisions to align it with international standards. Consequently, the Turkish Building Earthquake Code (TEC-2018) [3] was introduced on January 1, 2019, incorporating significant modifications in linear and nonlinear seismic analysis methodologies, including updates on earthquake ground motion levels, building-use classifications, soil classification systems, and design spectral acceleration coefficients.

A key distinction between TEC-2007 and TEC-2018 is the number and selection of earthquake ground motion records required for time-history analysis. Under TEC-2007, time-history analyses can be conducted using either a maximum of three ground motions or the average response of at least seven ground-motion records. However, TEC-2018 mandates a minimum of 11 ground motion records for nonlinear time-history analysis (NTHA) to ensure statistical reliability in seismic performance assessments. This requirement significantly enhances the accuracy of seismic demand estimation but also increases computational complexity, posing challenges for practical engineering applications.

Time-history analysis (THA) is one of the most reliable methods for evaluating the dynamic response of structures to earthquake loading. They are broadly categorized into linear time history analysis (LTHA) and nonlinear time history analysis (NTHA).

- The LTHA assumes linear elastic behavior, making it computationally efficient for evaluating the structural performance under different seismic input motions. Although it neglects material and geometric nonlinearities, LTHA provides a reliable first-order approximation of the seismic demand and serves as an effective tool for comparative analyses using real and artificial spectrum-matched ground-motion records. In the context of this study, the term “spectrum-matching methodologies” specifically refers to the generation and application of both real recorded and artificially synthesized earthquake motions that are matched to a target response spectrum, rather than general spectrum-scaling or modification procedures.
- In contrast, the NTHA incorporates inelastic deformations, plastic hinge formations, and progressive structural damage mechanisms, offering a more realistic representation of seismic behavior. However, NTHA requires significantly more computational resources owing to its iterative nature, the complexity of modeling nonlinear material properties, and the large deformation effects.

Although NTHA is essential for performance-based seismic design, it remains a widely used tool for preliminary evaluations, particularly in the context of spectrum-matching methodologies. The selection and transformation of earthquake ground motion records significantly influence both the LTHA and NTHA outcomes, particularly in base shear force estimation, structural response predictions, and displacement demands.

Accurately determining spectrum-matched earthquake ground-motion records is essential for structural analysis and performance-based design. In structural elements where plastic hinges are expected to form, the spectrum-matching process must account for the sectional properties at these hinge locations. If plastic hinges occur exclusively in the bending mode, the equilibrium equations must be reformulated after each hinge formation, thereby introducing additional unknowns and constraints that require an iterative approach. Linearization techniques offer an approximate solution methodology when nonlinear relationships exist between the internal forces and deformations [4–12].

Given these complexities, LTHA remains a practical approach for code-based seismic assessments, whereas NTHA is indispensable for capturing realistic nonlinear structural behavior. Future research should integrate advanced simulation platforms (e.g., OpenSees and Abaqus) to enhance spectrum-matching methodologies and improve the reliability of seismic demand estimation in performance-based earthquake engineering.

Recent studies on LTHA in structural engineering are relatively limited, particularly regarding their application to reinforced concrete (RC) structures. Most existing studies have been conducted within the framework of national standards, such as TEC-1975 [13], TEC-1998 [14], TEC-2007 [2], TEC-2018 [3], and the Istanbul Seismic Design Code for Tall Buildings [15], as well as international standards, such as the Uniform Building Code (UBC) [16, 17], Eurocode 8 (EC 8) [18], and various Federal Emergency Management Agency (FEMA) guidelines, including FEMA 222A [19], 223A [20], 302 [21], and 303 [22]. Furthermore, the

American Society of Civil Engineers (ASCE) has developed seismic provisions through ASCE/SEI 7-98 [23], 7-02 [24], 7-05 [25], 7-10 [26], and 7-16 [27], which have been widely adopted in the structural engineering field. Similarly, the International Building Code (IBC) [28] and alternative seismic analysis procedures, such as the Los Angeles Tall Buildings Structural Design Council (LATBSDC) guidelines [29], have influenced the development of seismic design methodologies. Despite these advancements, gaps remain in the comprehensive understanding of spectrum-matching methodologies and ground-motion selection strategies and their impact on seismic performance assessments. Therefore, further research is essential to address these limitations and refine seismic design methodologies to improve the accuracy and reliability of earthquake-resistant structures.

Recent comparative studies on steel and composite moment-resisting frames have highlighted the critical influence of spectrum selection, ground-motion scaling, and soil classification on the structural response and performance-based design. For instance, Etlı and Güneyisi [30] investigated the behavioral factors of composite buildings designed under different code provisions, whereas Etlı and Akgül [31] compared the seismic behaviors of steel–concrete composite buildings designed according to the TEC-2018 and international standards. Similarly, Etlı [32] evaluated the performance of composite structures in poorly graded soils, emphasizing the role of local soil effects on the seismic response variability. These studies complement the current research by reinforcing the importance of integrating soil–structure interactions and spectrum-matching effects into seismic design frameworks.

Currently, the Response Spectrum (RS) method (RSM) is one of the most widely used approaches for evaluating the seismic demands of structures. This method enables engineers to assess structural performance by analyzing spectral acceleration values across different vibration periods. In Fig. 1, the horizontal axis represents the natural vibration period ( $T$ ), which characterizes the fundamental period of a structure under seismic loading, whereas the vertical axis denotes the spectral acceleration

( $S_a$ ), which indicates the maximum acceleration response of the structure at a given period. According to TEC-2018, the reduced design response spectrum ( $S_{aR}$ ) is obtained by dividing the horizontal elastic spectral acceleration ( $S_{ae}$ ) by the seismic load reduction factor ( $R_a$ ) (Fig. 1(b), Curve 2-Green). In contrast, ASCE/SEI 7-16 modifies the design spectrum by applying the behavior coefficient ( $R$ ) (Fig. 1(c), Curve 3-Blue).

These different reduction factors resulted in variations in the seismic load estimations, as represented by the hatched area in Fig. 1. This area illustrates the difference between the elastic spectrum (ES) and reduced design spectra, highlighting the impact of code-specific reduction factors on seismic force predictions. The engineering significance of these reductions is critical for seismic-resistant designs. The reduction in the spectral acceleration values affects the base shear force calculations, directly influencing the structural performance. The ES ( $S_{ae}$ ) (Fig. 1(a), Curve 1-Red) provides a conservative estimate of seismic demand, whereas the TEC-2018 and ASCE reductions (Fig. 1(b) and Fig. 1(c)) allow for more economical yet structurally safe designs by incorporating ductility and energy dissipation effects. However, the extent of reduction differs among codes, potentially leading to variations in design outcomes.

The primary objective of this study is to quantify these differences and assess their implications for seismic performance. Three different spectrum types (ES, TEC-2018, and ASCE) are evaluated across four different soil classes (ZA-ZD) and three different structural heights (3-, 9-, and 20-story buildings).

The analyses employ LTHA using SAP2000® v.14.0.0 [33], incorporating seven different earthquake ground motion records and multiple lateral load combinations. This study primarily examines base shear responses to evaluate how spectrum-matching methodologies influence seismic design; displacement and interstory drift metrics are outside the present scope and are reserved for future work. To avoid scope creep and ensure statistical consistency across the

considered spectra and soil classes, only the base shear outputs are reported and discussed in detail.

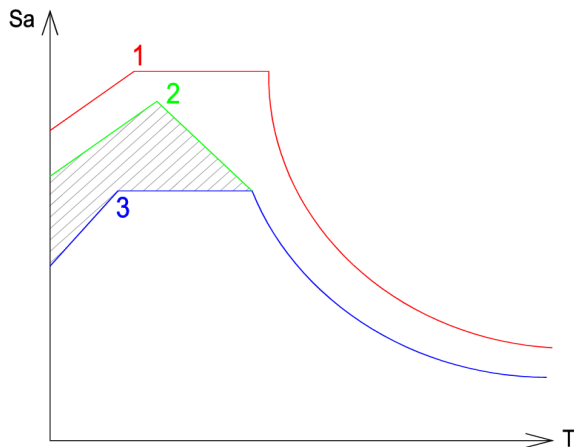


**Figure 1.** (a) Elastic spectrum ( $S_{ae}$ ) – shown in red, (b) TEC-2018 reduced design spectrum derived using the reduction factor  $R_a$  – shown in green, and (c) ASCE/SEI 7-16 reduced spectrum based on the response modification factor  $R$  – shown in blue

To improve predictive accuracy, future research should integrate NTHA and employ advanced simulation platforms, such as OpenSees or Abaqus, for a more refined evaluation of plastic hinge formations, material yielding, and progressive damage mechanisms. This study provides a quantitative framework for comparing seismic responses under different spectrum-matching conditions, thereby addressing critical gaps in performance-based seismic engineering. These findings are expected to contribute to seismic code development, spectrum-matching optimization, and enhanced reliability of earthquake-resistant structural design methodologies.

The remainder of this paper is organized as follows. Section 2 details the methodology, including the selection and processing of spectrum-matching parameters, seismic ground motion records, and the computational modeling techniques used. In addition, it provides a theoretical framework and governing equations for analysis. Section 3 outlines the structural modeling process, including the design parameters for the MRFs, SAP2000® software implementation, and optimization of structural sections. Section 4 focuses on the selection, scaling, and transformation of earthquake records, with an emphasis on spectrum compatibility and the challenges associated with

artificial versus natural ground motions. Section 5 presents a comprehensive evaluation of the analysis results, including base shear force comparisons, structural response variations across different soil conditions, and the influence of spectrum-matching techniques.

Finally, Section 6 summarizes the key findings, discusses their practical implications for seismic design, and provides recommendations for future studies. This study contributes to the advancement of seismic-resistant design methodologies by systematically assessing the impact of spectrum-matching parameters derived from real and artificial earthquake ground motions, thereby offering valuable insights to engineers and researchers in earthquake-prone areas.

## 2. Seismic Analysis Methodology Using Spectrum Matching Techniques

The design response spectrum prescribed by regulations is commonly used in the design of traditional structures. However, for more complex structures, an appropriate spectrum should be selected based on the seismic hazard levels, soil conditions, and structural characteristics. The acceleration response spectrum curve was obtained by summing the absolute values of the maximum acceleration of the earthquake ground motion applied to a single-degree-of-freedom (SDOF) system. To estimate the structural response, the behavior of a multi-degree-of-freedom (MDOF) system at any vibration period is compared with that of an SDOF system with the same vibration period [6].

A constant damping ratio ( $\zeta = 5\%$ ) was applied to ensure consistency and focus on the effects of the spectrum-matching parameters. However, varying the damping ratio can provide deeper insights into dynamic behavior, particularly for structures with distinct energy dissipation mechanisms. The motion equation of a nonlinear SDOF system subjected to an earthquake ground motion is expressed as follows: (1):

$$m\ddot{u} + c\dot{u} + f_s(u) = p(t) = -m\ddot{u}_g(t) \quad (1)$$

where:

- $m$  denotes the mass of the structure,
- $c$  denotes the damping coefficient (representing energy dissipation),
- $f_s(u)$  represents the internal restoring force,
- $p(t)$  is the external applied force, which in this case is due to earthquake ground acceleration  $\ddot{u}_g(t)$ ,
- $u$ ,  $\dot{u}$ , and  $\ddot{u}$  are the displacement, velocity, and acceleration of the structure, respectively

## 2.1. Time-integration approach using Newmark's method

The equation of motion in an LTHA is often solved using time-step numerical integration. Among these, Newmark's method is widely used for dynamic loading scenarios such as earthquake ground motion, vibration, and impact loading [34]. Newmark's method allows for numerical integration of SDOF and MDOF systems, and is typically applied in two variants (see step 4 in Fig. 2):

- Average constant acceleration method (middle-point rule)
- Linear acceleration method

For structural analysis, the average constant acceleration method is commonly used because of its stability. The numerical formulation of the Newmark integration scheme is given by Eqs. (2) and (3), respectively.

$$\dot{U}_{I+1} = \dot{u}_I + [(1 - \gamma)\Delta t]\ddot{u}_I + (\gamma\Delta t)\ddot{u}_{I+1} \quad (2)$$

$$u_{I+1} = u_I + (\Delta t)\dot{u}_I + [(0.5 - \beta)(\Delta t)^2]\ddot{u}_I + [\beta(\Delta t)^2]\ddot{u}_{I+1} \quad (3)$$

where,  $u_I$ ,  $\dot{u}_I$ , and  $\ddot{u}_I$  represent the displacement, velocity, and acceleration at time  $I$ , respectively, and  $u_{I+1}$ ,  $\dot{u}_{I+1}$ , and  $\ddot{u}_{I+1}$  represent the displacement, velocity, and acceleration at time  $I + 1$ , respectively.  $\Delta t$  is the time step [7].  $\gamma$  and  $\beta$  determine the stability and accuracy of the integration scheme. For unconditional stability, the standard Newmark coefficients are taken as  $\gamma = 1/2$  and  $\beta = 1/4$  which ensures that

numerical integration remains stable under seismic excitations.

## 2.2. Assumption of constant acceleration and motion equations

Newmark's method assumes that acceleration remains constant within each time step ( $\Delta t$ ), leading to the following numerical approximations, given in Eqs. (4) through (8) [34]:

$$\ddot{u}(\tau) = \frac{1}{2}(\ddot{u}_{i+1} + \ddot{u}_i) \quad (4)$$

$$\dot{u}(\tau) = \dot{u}_i + \frac{\tau}{2}(\ddot{u}_{i+1} + \ddot{u}_i) \quad (5)$$

$$\dot{u}_{i+1} = \dot{u}_i + \frac{\Delta t}{2}(\ddot{u}_{i+1} + \ddot{u}_i) \quad (6)$$

$$u(\tau) = u_i + \dot{u}_i\tau + \frac{\tau^2}{4}(\ddot{u}_{i+1} + \ddot{u}_i) \quad (7)$$

$$u_{i+1} = u_i + \dot{u}_i\Delta t + \frac{(\Delta t)^2}{4}(\ddot{u}_{i+1} + \ddot{u}_i) \quad (8)$$

where  $\tau$  represents the time interval affected by the impulse.

The Newmark average constant acceleration method offers a robust and widely accepted time integration scheme for the numerical solution of dynamic equilibrium equations for SDOF systems subjected to seismic loading. This method is based on the assumption that acceleration remains constant over a discrete time interval  $\Delta t$ , providing a stable and convergent basis for the time-stepping analysis.

Within this framework, the acceleration at any time step is approximated as the average of the accelerations at the beginning and end of the interval, enabling the quadratic interpolation of displacement and linear interpolation of velocity. This approach enhances both computational stability and accuracy, particularly for structural systems that experience significant dynamic excitations.

To represent realistic structural behavior under seismic conditions, the motion equations were formulated using a damping ratio  $\zeta = 0.05$ , in accordance with ASCE 7-22 [35], which recommends this value for ordinary structures.

For the Newmark integration parameters,  $\gamma=0.5$  and  $\beta=0.25$ . These parameters are known to ensure unconditional numerical stability and are particularly effective in simulating the seismic responses of elastic and moderately inelastic systems.

### 2.3. Numerical integration approach for seismic response calculation

In the Newmark linear acceleration method, it is assumed that acceleration remains constant during the time interval  $\Delta t$ , while in the Newmark average constant acceleration method, acceleration is assumed to vary linearly over the same interval. The numerical calculation steps for this method are presented in Eqs. (9)-(13):

$$\ddot{u}(\tau) = \ddot{u}_i + \frac{\tau}{\Delta t}(\ddot{u}_{i+1} - \ddot{u}_i) \quad (9)$$

$$\dot{u}(\tau) = \dot{u}_i + \ddot{u}_i\tau + \frac{\tau^2}{2\Delta t}(\ddot{u}_{i+1} - \ddot{u}_i) \quad (10)$$

$$\dot{u}_{i+1} = \dot{u}_i + \frac{\Delta t}{2}(\ddot{u}_{i+1} + \ddot{u}_i) \quad (11)$$

$$u(\tau) = u_i + \dot{u}_i\tau + \ddot{u}_i\frac{\tau^2}{2} + \frac{\tau^3}{6\Delta t}(\ddot{u}_{i+1} - \ddot{u}_i) \quad (12)$$

$$u_{i+1} = u_i + \dot{u}_i\Delta t + (\Delta t)^2\left(\frac{1}{6}\ddot{u}_{i+1} + \frac{1}{3}\ddot{u}_i\right) \quad (13)$$

By setting  $\gamma = 1/2$  and  $\beta = 1/6$  in Eqs. (2) and (3), a linear acceleration change is obtained. The complete time-stepping procedure using Newmark's method is shown in Table 1.

Thus, the Newmark method provides a robust and widely used integration scheme for THA in seismic applications, effectively balancing the numerical stability and computational efficiency.

Each step in Table 1 is iteratively solved until the full time-history response is obtained, ensuring the accuracy of the structural response calculations. Owing to its numerical stability, the Newmark method is well-suited for both LTHA and NTHA, making it the preferred approach in seismic engineering applications. This reliable numerical approach enables accurate seismic

response predictions, forming the foundation for developing a reduced design acceleration spectrum, which is essential for evaluating seismic demands in structural analysis.

**Table 1.** Calculation model developed using Newmark's method for time-stepping [34]

Special cases
(1) Average constant acceleration method $\left[\gamma = \frac{1}{2}, \beta = \frac{1}{4}\right]$
(2) Linear acceleration method $\left[\gamma = \frac{1}{2}, \beta = \frac{1}{6}\right]$
<b>1.0 Start</b>
1.1. $\ddot{u}_0 = \frac{p_0 - c\dot{u}_0 - ku_0}{m}$
1.2. $\Delta t$ seçilir
1.3. $\alpha_1 = \frac{1}{\beta(\Delta t)^2}m + \frac{\gamma}{\beta\Delta t}c;$ $\alpha_2 = \frac{1}{\beta\Delta t}m + \left(\frac{\gamma}{\beta} - 1\right)c;$ $\alpha_3 = \left(\frac{1}{2\beta} - 1\right)m + \Delta t\left(\frac{\gamma}{2\beta} - 1\right)c$
1.4. $\hat{k} = k + \alpha_1$
<b>2.0. Calculations at each step [<math>i = 0, 1, 2, \dots</math>]</b>
2.1. $\hat{p}_{i+1} = p_{i+1} + a_1u_i + a_2\dot{u}_i + a_3\ddot{u}_i$
2.2. $u_{i+1} = \frac{\hat{p}_{i+1}}{k}$
2.3. $\dot{u}_{i+1} = \frac{\gamma}{\beta\Delta t}(u_{i+1} - u_i) + \left(1 - \frac{\gamma}{\beta}\right)\dot{u}_i + \Delta t\left(1 - \frac{\gamma}{2\beta}\right)\ddot{u}_i$
2.4. $\ddot{u}_{i+1} = \frac{1}{\beta(\Delta t)^2}(u_{i+1} - u_i) - \frac{1}{\beta\Delta t}\dot{u}_i - \left(\frac{1}{2\beta} - 1\right)\ddot{u}_i$
<b>3.0 In the next step, <math>i</math> is replaced with <math>i + 1</math>, and the steps between 2.1 and 2.4 are repeated for the next step.</b>

### 2.4. Development of the reduced design acceleration spectrum for structural analysis

Recent updates in ASCE 7-22 [35] introduced a Multi-Period Design Response Spectrum, providing a more refined approach to seismic design by addressing the potential conservatism in spectral accelerations, particularly in regions with lower seismic activity, such as the Central and Eastern United States. The standard also

delineates methodologies such as the general procedure, ground motion hazard analysis, and dynamic situation response analysis, which enhance the precision of seismic hazard assessments by integrating site-specific effects into the design process.

Furthermore, the updated ASCE/SEI 41-23 [36] standard revises the analysis procedures for evaluating and retrofitting existing buildings to withstand seismic impacts, ensuring alignment with current seismic hazard models and improving performance-based assessment methods. Additionally, recent studies have emphasized the significance of SSI and site-specific soil conditions in seismic design, highlighting the necessity of incorporating accurate local soil effect factors into seismic design. These updates provide a comprehensive framework for developing reduced design spectra, thereby improving the reliability of seismic performance assessments and the resilience of structures under earthquake loading [37]. Recent studies have highlighted the importance of functional recovery in modern reinforced concrete buildings after earthquakes, emphasizing design strategies that enhance their structural resilience [38]. Additionally, self-centering beam systems in steel frame structures have demonstrated improved seismic performance through shaking table experiments and numerical analyses, further supporting the integration of advanced design methodologies for reducing the design acceleration spectra [39].

This section provides a structured approach for developing a reduced design acceleration spectrum for structural analysis, incorporating the seismic hazard definitions established by Türkiye's Disaster and Emergency Management Authority (AFAD). The geometric mean of the spectral acceleration coefficients in two orthogonal directions, represented by  $S_s$  (short-period spectral acceleration) and  $S_1$  (spectral acceleration at 1.0 sec period), forms the basis of spectral calculations [40, 41]. These values, normalized with respect to gravitational acceleration ( $g$ ), assume a reference site condition of  $V_s = 760 \text{ m/s}$  and a damping ratio of 5%. Using Eq. (14), the map spectral accelerations are converted into design spectral acceleration coefficients ( $S_{DS}$  and  $S_{D1}$ ) by

incorporating the local soil effect factors ( $F_s$  and  $F_1$ ). The horizontal elastic design spectral acceleration  $S_{ae}(T)$ , which varies with the natural vibration period ( $T$ ), is then determined using Eq. (15):

$$\begin{aligned} S_{DS} &= S_s F_s \\ S_{D1} &= S_1 F_1 \end{aligned} \quad (14)$$

$$\begin{aligned} S_{ae}(T) &= (0.4 + 0.6 \frac{T}{T_A}) S_{DS} & (0 \leq T \leq T_A) \\ S_{ae}(T) &= S_{DS} & (T_A \leq T \leq T_B) \\ S_{ae}(T) &= \frac{S_{D1}}{T} & (T_B \leq T \leq T_L) \\ S_{ae}(T) &= \frac{S_{D1} T_L}{T^2} & (T_L \leq T) \end{aligned} \quad (15)$$

The characteristic periods  $T_A$  and  $T_B$  of the design response spectrum for horizontal ground motion are expressed as functions of  $S_{DS}$  and  $S_{D1}$  in Eq. (16):

$$\begin{aligned} T_A &= 0.2 \frac{S_{D1}}{S_{DS}} \\ T_B &= \frac{S_{D1}}{S_{DS}} \end{aligned} \quad (16)$$

To determine reduced earthquake loads, the reduced design spectral acceleration  $S_{aR}(T)$  is calculated by dividing the elastic spectral acceleration  $S_{ae}(T)$  by the earthquake load reduction factor  $R_a(T)$ , as given in Eq. (17):

$$S_{aR}(T) = \frac{S_{ae}(T)}{R_a(T)} \quad (17)$$

TEC-2018 defines  $R_a(T)$  based on ductility capacity and force-based design principles, distinguishing between structures with  $T \leq T_B$  and  $T > T_B$ :

$$\begin{aligned} R_a(T) &= \frac{R}{I} & T > T_B \\ R_a(T) &= D + \left( \frac{R}{I} - D \right) \frac{T}{T_B} & T \leq T_B \end{aligned} \quad (18)$$

where  $I$  represents the importance factor,  $R$  is the structural system behavior factor, and  $D$  denotes the ductility factor used in seismic force reduction calculations. In this study, values for  $S_s$  and  $S_1$  were obtained from AFAD's Türkiye earthquake hazard maps, and the corresponding  $S_{DS}$  and  $S_{D1}$  coefficients were used to compute  $S_{aR}$  for different building models. The results were implemented using structural analysis software, and the elastic and reduced design acceleration spectra were compared.

The numerical comparison between the TEC-2018 and ASCE 7-22 design spectra, presented in Table 2, highlights the variations in spectral acceleration estimates across different vibration periods, emphasizing the influence of site-specific soil factors and ductility considerations on the seismic demand predictions. In the short-period range ( $T < 0.5s$ ), TEC-2018 shows slightly lower values than ASCE 7-22 (~3 – 8% reduction), implying less conservative seismic demands for rigid structures. For moderate-period buildings ( $0.5s < T < 2.0s$ ), the difference is minimal (~3 – 5%), suggesting similar force estimations under both codes.

**Table 2.** Comparison of ASCE 7-22 and TEC-2018 design spectra

Period ( $T$ ) [s]	ASCE 7- 22 $S_a(T)$ [g]	TEC-2018 $S_a(T)$ [g]	Difference (%)
0.2	1.20	1.10	-8.3%
0.5	0.85	0.82	-3.5%
1.0	0.60	0.58	-3.3%
2.0	0.35	0.33	-5.7%
3.0	0.25	0.22	-12.0%
4.0	0.18	0.16	-11.1%

However, in the long-period range ( $T > 2.0s$ ), TEC-2018 predicts significantly lower spectral accelerations, which may lead to reduced seismic demands for flexible structures compared with ASCE 7-22 (up to 12% lower).

The alternative spectra in this study were generated using Türkiye-based hypothetical seismic parameters to ensure a consistent comparison between the TEC-2018 and ASCE 7-16/22 provisions. Although the SAC Steel Project buildings (3-, 9-, and 20-story LA models defined in FEMA 355-C Appendix B) were adopted as benchmark geometries, their original

site definitions were not used. Instead, the local site conditions were re-defined according to TEC-2018 soil classes (ZA–ZD) and mapped to the equivalent ASCE site classes (A–E) using their corresponding  $(V_s)_{30}$  intervals. This adjustment was made to remove regional bias and enable an isolated assessment of the influence of the code-specific spectral formulations. This mapping enabled development of Elastic, TEC-2018 Reduced, and ASCE Reduced spectra under identical PGA and damping assumptions ( $\zeta = 5\%$ ), thereby allowing a direct and consistent code-to-code comparison. The resulting spectra represent hypothetical yet harmonized seismic conditions designed to isolate the influence of each code’s spectral reduction and soil-amplification formulations on the predicted base-shear demands. For clarity, the end-to-end workflow from model definition through record selection, spectrum matching, LTHA execution, and response extraction is summarized in Fig. 2.

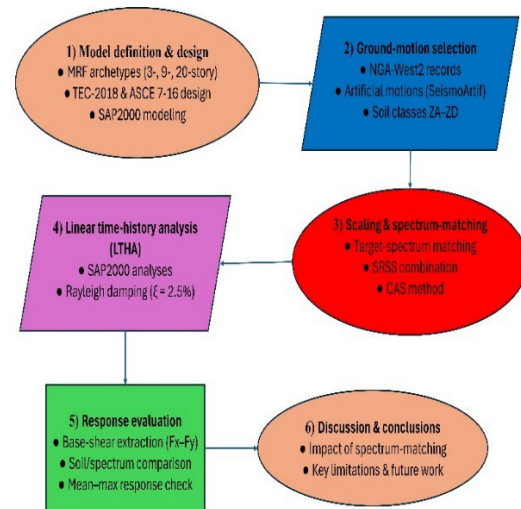


**Figure 2.** End-to-end workflow of the study

These findings reinforce the importance of advanced spectrum-matching techniques when applying the ASCE 7-22 provisions, particularly for tall buildings and performance-based seismic evaluations [35, 36]. Furthermore, ASCE/SEI 41-23’s emphasis on functional recovery and damping considerations is supported by these results, underscoring the need for enhanced damping models and stiffness degradation assessments in seismic design.

### 3. Computational Modeling and Structural Configuration of Steel Moment-Resisting Frames (MRFs)

MRFs are widely adopted in seismic design because of their superior ductility and energy dissipation capacity. This section details the computational modeling approach employed in this study, including the adopted structural configurations, design parameters, and finite element analysis (FEA) methodology.

#### 3.1. SAC steel project building models based on FEMA 355-C

The SAC Steel Project was developed in response to the structural failures observed during the 1994 Northridge earthquake. This project provides standardized benchmark models for evaluating the seismic performance of steel MRFs subjected to extreme loading conditions. These models incorporate nonlinear behavior, material yielding, and connection performance, making them suitable for advanced time-history analyses.

RSM is commonly used to assess the nonlinear behavior of structures, such as bridges. If the design spectrum values for the spectrum-matching earthquake records created from the recorded earthquake data exceed the standard values across all periods of the structure, three-dimensional (3D) time history records can be employed as a solution [42].

In this study, the SAC Steel Project model described in FEMA 355-C Appendix B [43] was utilized, and the sections of three-, nine-, and 20-story Los Angeles (LA) buildings were optimized for analysis using a moment-resisting steel-frame system. According to FEMA 355-C, the SAC Project developed structural models for three major seismically prone cities.

- **LA** (high seismicity region),
- **Seattle** (moderate seismicity region), and
- **Boston** (low seismicity region).

These buildings were designed according to the UBC [16], considering gravity, static, dynamic, and seismic loads. Each model represents a standard office building with stiff soil conditions, classified as Soil Type D according to ASCE/SEI 7-16 [27]. In the present study, only the post-optimization sections of the LA models were adopted for the analysis, as they represent the final code-conforming configurations of the ductile steel MRF systems defined in FEMA 355-C. The Seattle and Boston models were not included because this study aimed to ensure consistency under Türkiye-based hypothetical seismic conditions.

#### 3.1.1. Structural characteristics of Los Angeles (LA) buildings and adopted post-optimization sections

LA building models were initially developed in the SAC Project to reflect post-Northridge design improvements. However, in this study, the final post-optimization configurations defined in FEMA 355-C were adopted as the analytical basis for the study. These optimized sections incorporated enhanced beam-column connection details and improved energy dissipation capacity, representing the most code-conforming and realistic configurations of ductile steel MRFs. The geometric characteristics of the buildings, including their heights and MRF layouts, are shown in Figs. 3(a) and 3(b), respectively. The optimized cross-sectional properties for each building model are presented in Tables 3, 4, and 5, where the post-Northridge design is compared with the post-optimization modifications. The 20-story LA building underwent extensive optimization of its column and beam sections to improve its seismic performance. The modifications focused on reducing plastic hinge formation and enhancing ductility under extreme ground motion.

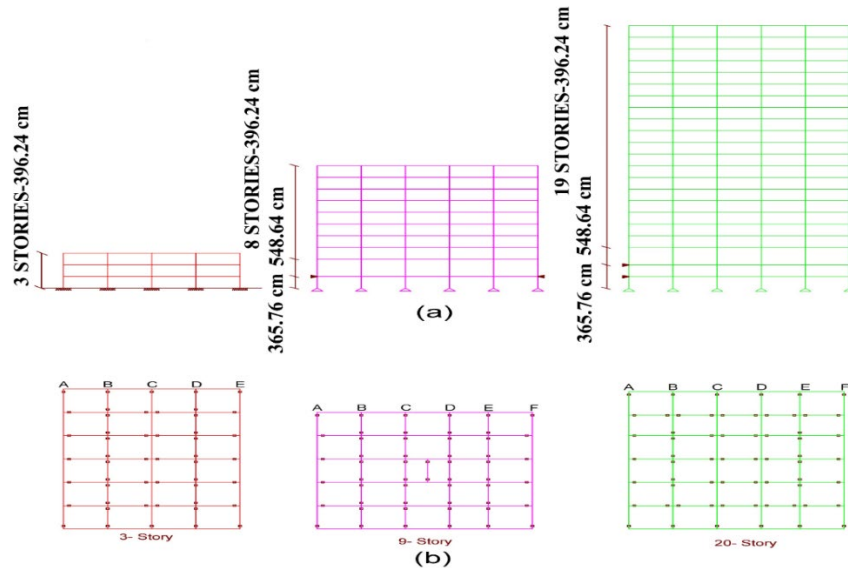


**Figure 3.** (a) Story heights for 3-, 9-, and 20-story LA buildings and (b) MRF layouts for model buildings

**Table 3.** Adopted post-optimization section properties for the 3-story LA building (FEMA 355-C)

Design for post-optimization				
Story	Exterior Column	Interior Column	Plate	Beam
1	W14x159	W14x159	0.0	W18x50, W18x65, W18x76
2	W14x159	W14x159	0.0	W18x50, W18x65, W18x76
3/Roof	W14x159	W14x159	0.0	W18x50, W18x65, W18x76

**Table 4.** Adopted post-optimization section properties for the 9-story LA building (FEMA 355-C)

Design for post-optimization				
Story	Exterior Column	Interior Column	Plate	Beam
-1	W14x176	W14x233	0.0	W18x35, W18x65, W18x71
1	W14x176	W14x233	0.0	W18x35, W18x65, W18x71
2	W14x176	W14x233	0.0	W18x35, W18x65, W18x71
3	W14x176	W14x233	0.0	W18x35, W18x65, W18x71
4	W14x132	W14x159	0.0	W18x35, W18x50, W18x60, W18x65
5	W14x132	W14x159	0.0	W18x35, W18x50, W18x60, W18x65
6	W14x132	W14x159	0.1/2	W18x35, W18x50, W18x60, W18x65
7	W14x132	W14x132	0.0	W18x35, W18x46, W18x55, W18x60
8	W14x132	W14x132	0.1/2	W18x35, W18x46, W18x55, W18x60
9/Roof	W14x132	W14x132	0.0	W18x35, W18x46, W18x55, W18x60

### 3.2. Structural design and finite element modeling (FEM) in SAP2000®

The structural design of the LA model buildings follows the Load and Resistance Factor Design (LRFD) method, which ensures that all structural components meet the required safety and performance criteria. Dynamic analyses were conducted using the LTHA under three distinct spectral definitions: ES, TEC-2018 Reduced Spectrum, and ASCE 7-16 Reduced Spectrum. For all the models, seven spectrum-compatible ground motions were employed, selected, and

scaled in accordance with both the TEC-2018 and ASCE/SEI 7-16 provisions. According to LRFD principles, the design strength ( $\phi R_n$ ) must be equal to or greater than the required strength ( $R_u$ ), as defined in Eq. (19) [44]:

$$R_u \leq \phi R_n \tag{19}$$

where:

- $R_u$  = required strength due to applied loads,
- $\phi R_n$  = design strength considering resistance factors.

The following key assumptions were considered in the numerical analysis of the three-, nine-, and 20-story buildings in Los Angeles.

- Material Properties:
  - The steel members conformed to ASTM A992 ( $F_y = 345\text{MPa}$ ,  $F_u = 450\text{MPa}$ ).
  - The beam-to-column connections were modeled as fully restrained (FR) moment connections.
- Gravity and seismic loading
  - Dead and live loads were applied according to seismic load provisions [27].
  - Seismic demands were computed using site-specific ground motion records and response spectrum analysis (RSA).
- Structural Behavior and Boundary Conditions
  - The column bases were assumed to be fully fixed to prevent rotational and translational movements.
  - The P- $\Delta$  effects were incorporated to account for the geometric nonlinearity.
  - Floor diaphragms are modeled as rigid diaphragms to maintain the in-plane stiffness and load redistribution capacity.

The finite element model was constructed using 3D frame elements with six degrees of freedom per node, enabling an accurate representation of axial, shear, and flexural deformations. A mesh discretization strategy was adopted, segmenting the beam and column elements into  $0.5\text{m} - 1.0\text{m}$  divisions to optimize computational efficiency and numerical stability. Although both ASCE 7-16 and TEC-2018 prescribe a minimum of 11 ground-motion records for nonlinear time-history analysis (NTHA), this requirement does not apply to linear time-history analysis (LTHA). In this study, seven spectrum-compatible records were adopted, which were consistent with the SAC Project benchmark framework and sufficient for elastic-range response evaluation.

The following seismic loading scenarios were considered:

- Site-specific response spectra for various soil conditions.
- Conducted using a scaled acceleration time series from PEER [45].
- Self-weight plus additional ASCE-prescribed dead and live loads.

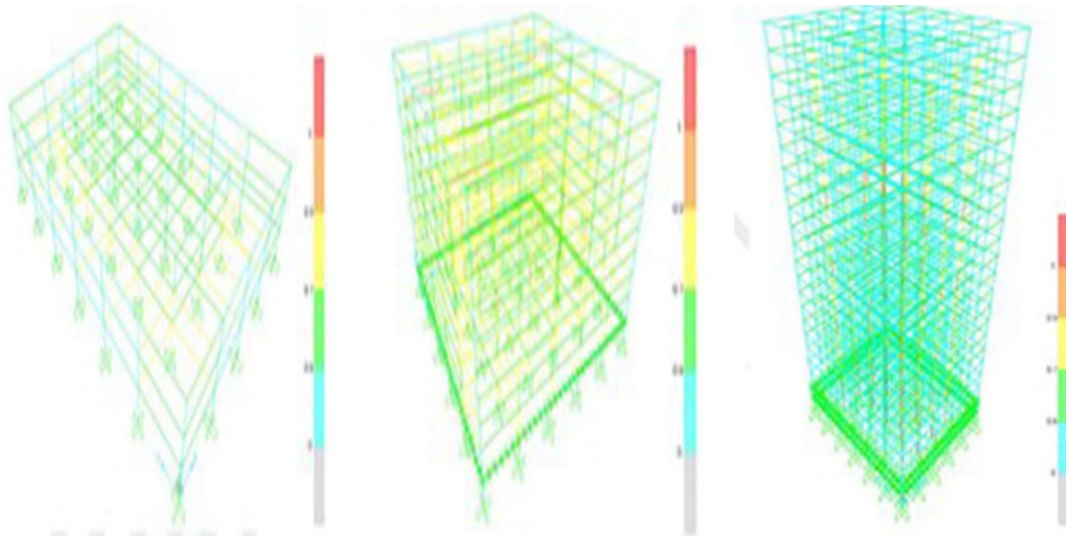
To model the energy dissipation mechanisms, Rayleigh damping with a damping ratio of 5% was assigned to the fundamental mode of vibration. To assess the seismic performance, SAP2000® steel design checks were conducted to compute the following:

- Axial Demand-to-Capacity Ratio ( $P_{Ratio}$ ): The ratio of applied axial force to the member's axial load capacity.
- Major Bending Moment Demand-to-Capacity Ratio ( $M_{MajRatio}$ ): The ratio of applied major-axis bending moment to the flexural capacity of the member.

The critical demand/capacity (D/C) ratios, including the axial force-bending moment interaction (PMM) ratios, were analyzed to identify potential overstressed members. The results for the three-, nine-, and 20-story LA buildings are shown in Figs. 4(a)–(c). The beam and column sections were not modified or re-optimized in this study. All numerical evaluations were performed on the final SAC-optimized geometries to ensure consistency across code-based spectral inputs. A PMM ratio greater than 1.0 indicates that a structural member has exceeded its design capacity, signifying an overstressed condition that may compromise the integrity of the building structure. The critical members that surpassed the allowable limits were identified and documented to validate the model reliability. The finite element model was validated to ensure its accuracy and numerical stability as follows.

**Table 5.** Adopted post-optimization section properties for the 20-story LA building (FEMA 355-C)

Story	Design for post-optimization			
	Exterior Column	Interior Column	Plate	Beam
-2	W14x193	W14x211	0.0	W16x40, W16x45
-1	W14x193	W14x211	0.0	W16x40, W16x45
1	W14x193	W14x211	0.0	W16x40, W16x45
2	W14x193	W14x211	0.0	W16x40, W16x45
3	W14x193	W14x211	0.0	W16x40, W16x45
4	W14x193	W14x211	0.0	W16x40, W16x45
5	W14x176	W14x193	0.0	W16x40, W16x45
6	W14x176	W14x193	0.0	W16x40, W16x45
7	W14x176	W14x193	0.0	W16x40, W16x45
8	W14x176	W14x193	0.0	W16x40, W16x45
9	W14x159	W14x176	0.0	W16x40, W16x45
10	W14x159	W14x176	0.0	W16x40, W16x45
11	W14x159	W14x176	0.0	W16x40, W16x45
12	W14x159	W14x176	0.0	W16x40, W16x45
13	W14x145	W14x159	0.0	W16x40, W16x45
14	W14x145	W14x159	0.5/8	W16x40, W16x45
15	W14x145	W14x159	0.5/8	W16x40, W16x45
16	W14x145	W14x159	0.5/8	W16x40, W16x45
17	W14x145	W14x159	0.5/8	W16x40, W16x45
18	W14x145	W14x159	0.5/8	W16x40, W16x45
19	W14x145	W14x159	0.1/2	W16x40, W16x45
20/Roof	W14x145	W14x159	0.0	W16x40, W16x45

**Figure 4.** D/C PMM ratios for (a) 3-story, (b) 9-story, and (c) 20-story LA buildings

- Fig. 4 illustrates the demand-to-capacity ratios (PMM interaction) for the adopted post-optimization sections under the applied dynamic loading. This figure serves as a pre-analysis verification of the model adequacy rather than a comparative design check.
  - Incremental mesh refinements were evaluated to assess the convergence of the peak interstory drift ratio.
  - The computed base shear values were verified using force-based seismic-demand prediction.
  - Fundamental vibration periods ( $T_1$ ,  $T_2$ , and  $T_3$ ) were compared with the theoretical estimates.
- This robust computational framework ensures a realistic and reliable representation of the seismic behavior of LA buildings, providing a foundation

for further structural performance evaluations and optimization strategies.

#### 4. Ground Motion Selection Scaling and Transformation in Seismic Design

The accuracy of time-history seismic analysis depends heavily on the appropriate selection, scaling, and transformation of earthquake ground motions. Recent studies have highlighted that spectrum-matched artificial records, while improving agreement with a target response spectrum, may distort other intensity measures, such as strong-motion duration and cumulative energy content, potentially biasing structural response estimates. Foundational studies have discussed these trade-offs and provided guidance for record selection, scaling, and matching in performance-based analyses (e.g., [46–51]). Consistent with the literature, the present study treats artificial and real records as complementary inputs: artificial records for spectral consistency in elastic assessments and real records to capture the variability in

frequency content and phase characteristics. The selection criteria should consider site-specific soil conditions, proximity to the earthquake source, seismic intensity, and spectral compatibility. The ground motion records used in this study were selected from the PEER NGA-West2 [42] database using a set of clearly defined seismological parameters reported in Kulak [52]. The selection process employed a strike-slip fault mechanism, magnitude range of 4.8–7.5, source-to-site distances between 10 and 100 km, and shear-wave velocities  $(V_s)_{30}$  between 360 and 760 m/s. A total of seven real earthquake records were chosen for each soil classification (ZA–ZD), ensuring spectrum compatibility and statistical consistency. These criteria were defined to align with the TEC-2018 and ASCE 7-16 recommendations for performance-based design. Table 6 presents the principal features of the selected records, including the event name, recording station, year, magnitude,  $(V_s)_{30}$  value, and source-to-site distance.

**Table 6.** Key characteristics of selected real and artificial ground-motion records from the PEER NGA-West2 database [45]

No	Earthquake	Station	Year	Mw	$(V_s)_{30}$ (m/s)	Source Distance (km)
1	Morgan Hill	Gilroy Array #1	1984	6.19	1428	14.9
2	Düzce (Türkiye)	Lamont 1060	1999	7.14	782	25.8
3	Chi-Chi Taiwan-04	CHY102	1999	6.20	804	39.3
4	Chi-Chi Taiwan-04	TTN042	1999	6.20	845	68.9
5	Tottori Japan	HYG007	2000	6.61	760	99.6
6	Kocaeli (Türkiye)	Maslak	1999	7.51	446	53.0
7	Landers (USA)	Coolwater	1992	7.28	353	19.7

Note: The full dataset containing detailed ground-motion characteristics for all soil classifications (ZA–ZD), including additional PEER NGA-West2 records and scaling parameters, is provided in Kulak [52]. Artificial records were generated to match the target spectra for each soil class.

This section details the methodology used to select and scale natural and artificial earthquake records in accordance with the TEC-2018 [3] and ASCE/SEI 7-16 standards. In this study, the term “spectrum matching parameters” denotes not only the classification between real and artificial records, but also the frequency- and amplitude-adjustment coefficients, scaling factors, and phase-modification constraints applied to align the input ground motions with the target design spectrum. These parameters govern the level of spectral conformity and directly influence the variability of the structural response outcomes.

The primary variable in selecting earthquake records is soil classification, as it directly influences the dynamic response of structures. In this study, natural and artificial ground motions were selected for four local soil classes (ZA, ZB, ZC, and ZD) in TEC-2018. The following criteria were considered during selection:

- Ground motions were selected to match the local soil classifications (ZA-ZD).

- To observe near-field seismic effects, earthquake records were selected based on a source-to-site distance of 10–100 km, as determined through sensitivity analyses.
- Ground motions from seismic events with magnitudes ranging from 4.0 to 8.0 were used to ensure the inclusion of high-intensity earthquakes.

Natural earthquake records were obtained from the Pacific Earthquake Engineering Research Center (PEER) database [45, 53]. Artificial records were generated using the SeismoArtif software [54], which produces spectrum-compatible synthetic accelerograms by matching a specified target response spectrum using advanced computational algorithms. Ground motion scaling was performed to achieve spectral consistency with the target design spectrum while maintaining the physical characteristics of real earthquakes. The following steps were performed:

- The square root of the sum of squares (SRSS) method was used to obtain a composite response spectrum from the two horizontal components of each earthquake record.
- The spectral scaling factors were determined such that the amplitude ratio of the composite spectrum of selected records to the design spectrum over the  $0.2T_p - 1.5T_p$  period range was not less than 1.3, where  $T_p$  represents the dominant natural vibration period of the structure in the analyzed direction.
- Identical scaling factors were applied to both horizontal components of each record to maintain spectral integrity.
- To reduce scattering in the response results, conditioned average spectra (CAS) were used to refine the spectral compatibility by aligning the ground motions with site-specific earthquake characteristics (step 3 in Fig. 2).

To ensure spectral compatibility with the design spectrum, the earthquake records were transformed and modified while preserving the essential frequency content and amplitude characteristics of the actual ground motions. The

final selected records satisfy the requirement that the average spectral ordinates should not be lower than the design spectrum at any period. This study did not include SSI effects because the primary focus was on spectrum-matching parameters and soil classifications. Although SSI, varying damping ratios, and material property uncertainties significantly affect seismic behavior, their influence is most pronounced in soft soil conditions and in highly flexible structures. Future studies should incorporate SSI effects, advanced damping models, and material uncertainties to provide a more comprehensive understanding of the structural behavior under actual earthquake conditions. Although artificial ground motions closely match the target design spectrum, they may not fully represent the complex variability of actual seismic events. This observation is consistent with prior reports that emphasized potential distortions in duration and cumulative energy metrics following spectral matching [47–48, 55].

## 5. Seismic Performance Evaluation of Steel Structures Under Spectrum Matched Earthquake Records

The analysis stage in Fig. 2 (steps 4 and 5) was implemented for the ES, TEC-2018, and ASCE spectra across four soil classifications (ZA–ZD) and three steel moment-resisting frame configurations (3-, 9-, and 20-story). In the present study, the linear analysis method was used in time-history to solve 3-, 9-, and 20-story buildings for 3 different spectra, 4 different soil types (ZA-ZB-ZC-ZD) and 7 different earthquake records. In a model, there are a total of 252 earthquake records, including 84 earthquake records for x-direction and 84 earthquake records for y-direction from natural earthquakes, and 84 earthquake records in both directions from artificial earthquakes.

The results obtained from the natural and artificial earthquake records are detailed in Kulak [52]. The first period of the structure and the first period at which the mass participation ratio exceeds 90% in both directions (x–y) was obtained as 0.947. The damping ratio was assumed to be 2.5% [56]. The target design spectra defined in TEC-2018 and ASCE 7-16

correspond to a 5% damping ratio; therefore, they were not regenerated for 2.5% damping. Instead, the structural models in SAP2000 were analyzed using a 2.5% modal damping ratio to represent the lower inherent energy dissipation capacity of the steel moment-resisting frames, consistent with the recommendations of Kulak [52]. In line with the study objective, the results presented in Sections 5.1–5.3 are limited to the base shear (mean and maximum) for each spectrum–soil–height combination only. Displacement and inter-story drift outputs, which are important for performance-based assessments, are not reported herein and will be addressed in a subsequent study.

### **5.1. Behavior of LA buildings based on natural earthquake records**

The base shear force results of the 3-story building in the THA were calculated separately for the mean/average and maximum values in  $x$  – and  $y$  – directions, according to the soil classes. The base shear forces of the buildings according to ES, TEC-2018, ASCE, and RS for the ZA soil class are listed in Table 7. To validate the scaling procedure, the mean response spectra of the scaled ground motions were compared with the design spectrum. This comparison confirms the alignment across the period range of interest, demonstrating the reliability of the spectrum-matching methodology.

Minor variations reflecting natural seismic variability were observed but did not affect the consistency of the analysis results. The linear analysis base shear force results of the 9-story and 20-story buildings within a certain time interval are presented in Tables 8 and 9, for  $x$  – and  $y$  – directions, respectively, with the average and maximum values for different soil classes. A linear analysis was chosen in this study because of its computational efficiency and ability to provide a first-order understanding of the structural behavior under seismic loads. However, this approach may not capture the effects of material and geometric nonlinearities, particularly under severe seismic conditions. These limitations suggest the need for nonlinear analysis in future studies to assess the accuracy and reliability of the findings presented here.

### **5.2. Behavior of LA buildings based on artificial earthquake records**

The linear analysis base shear force results of a 3-story building within a certain time interval have been calculated for  $x$  – and  $y$  – axes, considering different soil classes. The base shear force results for soil classes ZA, ZB, ZC, and ZD are presented in Table 10, which shows the average and maximum values. The linear analysis base shear force results of 9-story and 20-story buildings, within a certain time interval, are presented in Tables 11 and 12 for  $x$  – and  $y$  – directions, respectively, with the average and maximum values for different soil classes. The results presented in Tables 7–12 clearly demonstrate the differences between the real and artificial earthquake records in estimating the base shear forces for various soil classifications. Although artificial records exhibit a more uniform spectral match and predictable structural response, real earthquake records introduce greater variability owing to their natural frequency and phase characteristics.

This variability is particularly pronounced in softer soil conditions (ZC, ZD), where deviations of up to  $\pm 35\%$  are observed. These findings highlight the need for a balanced approach for selecting ground-motion records for seismic analysis. In the following section, a detailed discussion of these results is provided, focusing on their engineering implications and practical applications in seismic-resistant structural design.

## **6. Results and discussion**

The analysis highlights the significant impact of spectrum-matching parameters on structural responses, emphasizing the need to select appropriate ground-motion records based on the intended application. Artificial earthquake records offer a more consistent and controlled spectral match that is closely aligned with the target design spectrum, particularly under stiffer soil conditions (ZA and ZB soil types).

**Table 7.** Base shear force results from LTHA of the 3-story steel MRF under different soil classifications (ZA, ZB, ZC, ZD)

Soil Type	Directions	Base Shear Force (kN)			
		ES	TEC-2018	ASCE	RS
ZA	ZA-Fx-mean	1025.20	1283.00	1147.90	1774.40
	ZA-Fx-max	1430.70	1746.20	1613.40	1774.40
	ZA-Fy-mean	913.20	1162.20	1180.30	1675.50
	ZA-Fy-max	1182.60	1745.40	1612.80	1675.50
ZB	ZB-Fx-mean	1001.20	1268.10	1237.10	1784.20
	ZB-Fx-max	1494.50	1593.60	1683.70	1784.20
	ZB-Fy-mean	1010.50	1065.10	1124.50	1686.00
	ZB-Fy-max	1501.00	1777.90	1683.20	1686.00
ZC	ZC-Fx-mean	2079.80	2328.20	2773.00	3295.60
	ZC-Fx-max	3167.10	3802.40	4723.50	3295.60
	ZC-Fy-mean	2188.70	1722.00	1763.90	3104.90
	ZC-Fy-max	2904.70	3130.30	2043.10	3104.90
ZD	ZD-Fx-mean	2315.20	3364.80	3139.50	4122.50
	ZD-Fx-max	4118.40	4583.80	3568.30	4122.50
	ZD-Fy-mean	1673.20	2522.20	2560.50	3879.10
	ZD-Fy-max	2767.60	4557.90	3448.90	3879.10

In contrast, actual earthquake records introduce greater variability owing to their inherent frequency content and phase characteristics, which lead to fluctuations in the base shear forces. This effect is particularly pronounced in softer soil types (ZC and ZD), where the base shear values from the real records show deviations of up to  $\pm 35\%$  compared with the artificial records, as evidenced by the dispersion ranges reported in Tables 7–12. Despite their

stability, artificial records may not fully capture the nonlinear effects of ground motions, which are essential for performance-based seismic assessments. Although artificial records are beneficial for preliminary design validation because of their uniformity, real earthquake records are indispensable for capturing realistic seismic uncertainties and variations in structural demand.

**Table 8.** Base shear force results from the LTHA of the 9-story steel MRF under different soil classifications (ZA, ZB, ZC, ZD)

Soil Type	Directions	Base Shear Force (kN)			
		ES	TEC-2018	ASCE	RS
ZA	ZA-Fx-mean	463.90	448.70	469.30	648.40
	ZA-Fx-max	727.70	751.20	761.20	648.40
	ZA-Fy-mean	434.70	424.80	488.60	716.80
	ZA-Fy-max	630.50	600.50	608.50	716.80
ZB	ZB-Fx-mean	463.90	535.00	464.00	648.80
	ZB-Fx-max	727.70	903.80	751.20	648.80
	ZB-Fy-mean	434.70	376.20	445.20	717.00
	ZB-Fy-max	630.50	599.20	600.50	717.00
ZC	ZC-Fx-mean	849.20	998.80	905.20	1212.30
	ZC-Fx-max	1149.90	1399.90	1037.90	1212.30
	ZC-Fy-mean	911.60	854.30	1249.60	1345.50
	ZC-Fy-max	1298.10	1455.20	1598.60	1345.50
ZD	ZD-Fx-mean	1285.70	968.20	1157.40	1528.90
	ZD-Fx-max	1549.70	1219.30	1419.30	1528.90
	ZD-Fy-mean	1006.90	897.80	1020.30	1698.50
	ZD-Fy-max	1426.70	1678.10	1574.20	1698.50

**Table 9.** Base shear force results from the LTHA of the 20-story steel MRF under different soil classifications (ZA, ZB, ZC, ZD)

Soil Type	Directions	Base Shear Force (kN)			
		ES	TEC-2018	ASCE	RS
ZA	ZA-Fx-mean	688.20	529.10	685.30	939.90
	ZA-Fx-max	1122.90	809.10	1317.30	939.90
	ZA-Fy-mean	628.90	630.50	658.40	975.30
	ZA-Fy-max	1332.80	815.10	823.90	975.30
ZB	ZB-Fx-mean	688.20	612.10	529.10	940.40
	ZB-Fx-max	1122.90	1159.20	809.10	940.40
	ZB-Fy-mean	628.90	531.70	630.50	975.60
	ZB-Fy-max	1332.80	814.60	815.10	975.60
ZC	ZC-Fx-mean	1290.90	884.30	1050.10	1760.80
	ZC-Fx-max	1848.10	1395.20	1540.20	1760.80
	ZC-Fy-mean	1097.90	1349.20	1609.20	1826.50
	ZC-Fy-max	1431.90	1718.30	2072.90	1826.50
ZD	ZD-Fx-mean	1340.00	1180.10	1105.80	2223.20
	ZD-Fx-max	2036.50	2501.20	1632.00	2223.20
	ZD-Fy-mean	1642.30	1725.60	1421.60	2312.80
	ZD-Fy-max	2140.10	2837.20	1957.60	2312.80

These findings emphasize that although code-based design validation can benefit from artificial records, real earthquake records should be prioritized for advanced seismic performance evaluations, particularly for structures on softer soils, where seismic demands exhibit higher variability.

The reliability of the adopted spectrum-matching methodology is corroborated by the consistent trends observed across the ES, TEC-2018 Reduced, and ASCE 7-16 Reduced spectra when

comparing base-shear outcomes obtained from both real and artificial record sets. Tables 7–12 collectively illustrate these trends across soil classes (ZA–ZD) and building heights, providing a transparent numerical basis for the comparative assessment without the need for additional graphical representation. Thus, the tabulated results guide engineers in making informed and code-consistent decisions regarding seismic-resistant designs.

**Table 10.** Base shear force results from the LTHA of the 3-story steel MRF subjected to artificial earthquake records across different soil classifications (ZA, ZB, ZC, ZD)

Soil Type	Directions	Base Shear Force (kN)			
		ES	TEC-2018	ASCE	RS
ZA	ZA-Fx-mean	1826.60	1993.80	1946.90	1774.40
	ZA-Fx-max	2111.70	2428.50	2314.30	1774.40
	ZA-Fy-mean	1847.90	2027.80	1998.10	1675.50
	ZA-Fy-max	2212.50	2628.70	2545.80	1675.50
ZB	ZB-Fx-mean	1825.00	2005.40	1953.70	1784.20
	ZB-Fx-max	2127.50	2341.70	2251.70	1784.20
	ZB-Fy-mean	1893.00	2005.80	1984.70	1686.00
	ZB-Fy-max	2265.60	2555.60	2489.40	1686.00
ZC	ZC-Fx-mean	3381.50	3763.90	3689.30	3295.60
	ZC-Fx-max	3962.10	4446.50	4271.10	3295.60
	ZC-Fy-mean	3487.80	3857.90	3701.00	3104.90
	ZC-Fy-max	4018.60	4803.10	4617.90	3104.90
ZD	ZD-Fx-mean	4193.70	4644.60	4507.70	4122.50
	ZD-Fx-max	4893.70	5526.50	5237.70	4122.50
	ZD-Fy-mean	4329.30	4762.30	4672.60	3879.10
	ZD-Fy-max	4815.60	5699.90	5453.40	3879.10

**Table 11.** Base shear force results from the LTHA of the 9-story steel MRF subjected to artificial earthquake records across different soil classifications (ZA, ZB, ZC, ZD)

Soil Type	Directions	Base Shear Force (kN)			
		ES	TEC-2018	ASCE	RS
ZA	ZA-Fx-mean	718.20	765.60	780.20	648.40
	ZA-Fx-max	866.30	883.60	899.20	648.40
	ZA-Fy-mean	714.00	722.70	753.10	716.80
	ZA-Fy-max	838.20	857.30	851.40	716.80
ZB	ZB-Fx-mean	730.50	768.80	782.10	648.80
	ZB-Fx-max	837.90	878.00	889.40	648.80
	ZB-Fy-mean	713.00	727.50	741.10	717.00
	ZB-Fy-max	841.30	881.50	863.40	717.00
ZC	ZC-Fx-mean	1343.80	1451.10	1415.30	1212.30
	ZC-Fx-max	1559.60	1656.70	1666.10	1212.30
	ZC-Fy-mean	1359.80	1402.90	1390.30	1345.50
	ZC-Fy-max	1660.50	1618.10	1608.40	1345.50
ZD	ZD-Fx-mean	1703.40	1752.10	1785.70	1528.90
	ZD-Fx-max	2074.40	2116.80	2126.50	1528.90
	ZD-Fy-mean	1656.60	1793.40	1788.70	1698.50
	ZD-Fy-max	1897.70	2048.50	2048.50	1698.50

**Table 12.** Base shear force results from the LTHA of the 20-story steel MRF subjected to artificial earthquake records across different soil classifications (ZA, ZB, ZC, ZD)

Soil Type	Directions	Base Shear Force (kN)			
		ES	TEC-2018	ASCE	RS
ZA	ZA-Fx-mean	890.70	974.20	1043.90	939.90
	ZA-Fx-max	952.80	1171.70	1342.40	939.90
	ZA-Fy-mean	949.30	1022.10	1084.20	975.30
	ZA-Fy-max	1014.60	1154.90	1387.20	975.30
ZB	ZB-Fx-mean	962.00	1002.90	1028.00	940.40
	ZB-Fx-max	1155.20	1178.50	1354.40	940.40
	ZB-Fy-mean	999.50	1027.70	1064.50	975.60
	ZB-Fy-max	1192.70	1184.70	1389.30	975.60
ZC	ZC-Fx-mean	1957.30	1834.20	1888.30	1760.80
	ZC-Fx-max	2444.90	2224.80	2250.60	1760.80
	ZC-Fy-mean	2011.60	1892.90	1950.80	1826.50
	ZC-Fy-max	2565.70	2185.40	2349.80	1826.50
ZD	ZD-Fx-mean	2268.90	2417.20	2439.50	2223.20
	ZD-Fx-max	3216.70	3020.80	3409.10	2223.20
	ZD-Fy-mean	2350.20	2506.50	2525.80	2312.80
	ZD-Fy-max	3329.50	3169.60	3515.20	2312.80

## 7. Conclusions and Engineering Implications for Seismic Resistant Structural Design

This study investigated the effects of the spectrum-matching parameters on the LTHA of steel MRFs. The findings demonstrate that the selection and transformation of earthquake ground motions significantly influence the seismic demand estimation and structural response predictions. The key conclusions and

their implications for seismic-resistant structural design are summarized as follows:

- The use of real earthquake records in The LTHA introduces variability in the base shear results, with fluctuations ranging from  $\pm 10\%$  to  $35\%$ , particularly for structures built on softer soil types (ZC and ZD). This variability highlights the inherent uncertainties in real ground motion and their impact on structural responses.

- Artificial earthquake records, when properly spectrum-matched to the target design spectrum, provide consistent and reliable structural response predictions with reduced variability in the base shear values. This consistency renders artificial records more suitable for preliminary design validation and code-based compliance testing.
- The observed scatter in the base shear forces from actual earthquake records suggests that the NTHA is more appropriate when natural ground motions are used, particularly to meet the TEC-2018 requirements. However, because the present study focuses on LTHA, the observed variability is discussed within the elastic response framework.
- Even when carefully selected, actual earthquake records do not perfectly match the design spectrum, leading to deviations in the structural response predictions. This emphasizes the importance of selecting earthquake records that closely align with the target design spectrum to ensure accurate seismic demand estimation.
- For cases requiring nonlinear analysis, real earthquake records provide a more realistic representation of seismic demand, particularly for structures subjected to material and geometric nonlinearities. However, this approach significantly increases the computational complexity, particularly when at least 11 earthquake records are used, as mandated by TEC-2018. In contrast, for linear time-history analysis (LTHA), where the structural behavior remains within the elastic range, the adoption of seven spectrum-compatible records, as used in this study, is sufficient to capture comparative spectral response trends while maintaining computational efficiency. This distinction between NTHA and LTHA clarifies that the present study complies with the code provisions for elastic response assessment while contextualizing the nonlinear requirements of TEC-2018.
- In soft soil conditions (ZC and ZD), the base shear values from real earthquake records exhibited the highest variability, suggesting that nonlinear analysis should be prioritized in these cases to prevent the underestimation of seismic demand.
- Engineering codes should differentiate between spectrum-matched artificial records, which are effective for design validation, and real earthquake records, which are necessary for performance-based seismic assessments to account for realistic ground motion uncertainty.
- This study confirms that although artificial earthquake records provide a stable and controlled input for seismic design, real earthquake records remain essential for capturing the complex and dynamic nature of structural behavior under earthquake loading. These findings reinforce the need for a balanced approach that integrates both types of records to optimize seismic risk assessments and ensure resilient structural designs. Future research should extend these findings by incorporating advanced SSI models, integrating machine learning-based predictive frameworks, and refining seismic hazard mapping techniques to enhance the accuracy of seismic demand assessments. These advancements further support the development of performance-based seismic design methodologies and ensure the robustness and reliability of the structures in earthquake-prone regions.

### 7.1. Future research directions and extensions

This study has certain limitations that define the scope of its findings and provide a foundation for future research. The analysis was restricted to linear time-history analysis (LTHA); thus, nonlinear phenomena such as material yielding, plastic hinge formation, and progressive stiffness degradation were not modeled. In addition, the use of a constant 2.5% Rayleigh damping ratio may not fully capture the range of damping characteristics encountered in real structures at different excitation levels. The selected record set, although matched to the target spectra, was limited in number and magnitude range and may not fully represent the stochastic variability of real earthquakes. Furthermore, SSI and 3D dynamic effects, which can influence the

dynamic response and base shear distribution in flexible or soft soil conditions, were not incorporated.

Building on these limitations, future research should prioritize refining spectrum-matching methodologies and explore their influence on seismic performance assessments by addressing the following critical gaps.

- Incorporating nonlinear time-history analysis (NTHA) to simulate yielding, plastic-hinge development, and damage evolution
- Multiple damping ratios (e.g., 2%, 5%, and 10%) in accordance with ASCE 7-22 to capture realistic energy dissipation characteristics.
- The structural responses under real and artificial ground motions were compared to quantify the discrepancies in the seismic demand.
- The ground motion dataset was expanded to cover a wider range of magnitudes (M4.0–M8.0), source-to-site distances (10–100 km), and soil profiles for statistical robustness.
- Enhancing spectrum-matching algorithms through sensitivity analyses addressing soil class and structural period effects
- Integration of SSI modeling using 3D finite element simulations for realistic ground-compliance representation
- Real-case validation of mid-rise steel MRFs in seismically active Turkish regions to bridge theoretical modeling and engineering practice.
- Extending the framework to reinforced concrete (RC) and composite systems to generalize applicability; and
- Cost-benefit analyses were performed to evaluate the trade-offs among computational demand, design precision, and economic feasibility.

Collectively, these advancements will strengthen performance-based earthquake engineering methodologies and contribute to the development of resilient, sustainable, and economically viable seismic-design strategies.

## Article Information Form

### *The Declaration of Conflict of Interest/ Common Interest*

No conflict of interest or common interest has been declared by authors.

### *Author Contributions*

Conceptualized the research framework, supervised the study, and coordinated the manuscript preparation: Ç.A.K.; Performed spectrum matching analysis and contributed to interpreting the results: K.T.; Conducsoil ted-structure interaction modeling and provided critical technical insights: K.P.; Contributed to data collection and preprocessing and assisted in figure preparation: M.K. All the authors have reviewed and approved the final version of the manuscript.

### *Artificial Intelligence Statement*

No artificial intelligence tools were used to write this article.

### *Copyright Statement*

Authors own the copyright of their work published in the journal and their work is published under the CC BY-NC 4.0 license.

## References

- [1] Z. Celep, *Introduction to Earthquake Engineering and Earthquake-Resistant Structural Design*, Istanbul, Turkey: Beta Publishing, 2022.
- [2] Specifications for Buildings to be Built in Seismic Areas (Turkish Earthquake Code), TEC-2007, Ankara, Turkey, 2007.
- [3] Turkish Building Earthquake Code, TEC-2018, Ankara, Turkey, 2018.
- [4] B. Borzi, G. M. Calvi, A. S. Elnashai, E. Faccioli, and J. J. Bommer, "Inelastic spectra for displacement-based seismic design," *Soil Dyn. Earthq. Eng.*, vol. 21, no. 1, pp. 47–61, Jan. 2001, doi: 10.1016/S0267-7261(00)00075-0. [Online]. Available: [https://doi.org/10.1016/S0267-7261\(00\)00075-0](https://doi.org/10.1016/S0267-7261(00)00075-0)

- [5] A. K. Chopra and R. K. Goel, "A modal pushover analysis procedure for estimating seismic demands for buildings," *Earthq. Eng. Struct. Dyn.*, vol. 31, no. 3, pp. 561–582, Mar. 2002, doi: 10.1002/eqe.144. [Online]. Available: <https://doi.org/10.1002/eqe.144>
- [6] A. K. Chopra, *Dynamics of Structures: Theory and Applications to Earthquake Engineering*, 3rd ed. Upper Saddle River, NJ, USA: Pearson Education, 2007.
- [7] A. K. Chopra, "Elastic response spectrum: a historical note," *Earthq. Eng. Struct. Dyn.*, vol. 36, no. 1, pp. 3–20, Jan. 2007, doi: 10.1002/eqe.609. [Online]. Available: <https://doi.org/10.1002/eqe.609>
- [8] R. Riddell, "Inelastic response spectrum: Early history," *Earthq. Eng. Struct. Dyn.*, vol. 37, no. 10, pp. 1175–1187, Jul. 2008, doi: 10.1002/eqe.810. [Online]. Available: <https://doi.org/10.1002/eqe.810>
- [9] M. Safar and A. Ghobarah, "Inelastic response spectrum for simplified deformation-based seismic vulnerability assessment," *J. Earthq. Eng.*, vol. 12, no. 2, pp. 222–248, Mar. 2008, doi: 10.1080/13632460701457272. [Online]. Available: <https://doi.org/10.1080/13632460701457272>
- [10] M. Zamora and R. Riddell, "Elastic and inelastic response spectra considering near-fault effects," *J. Earthq. Eng.*, vol. 15, no. 5, pp. 775–808, May 2011. doi: 10.1080/13632469.2011.555058. [Online]. Available: <https://doi.org/10.1080/13632469.2011.555058>
- [11] A. K. Chopra, *Dynamics of Structures: Theory and Applications to Earthquake Engineering*, 4th ed. Upper Saddle River, NJ, USA: Pearson Prentice Hall, 2012.
- [12] D. Ozturk and K. B. Bozdogan, "Nonlinear analysis of structures using inelastic spectrum," *Int. J. Technol. Sci.*, vol. 5, no. 3, pp. 49–55, Sep. 2013. [Online]. Available: <https://dergipark.org.tr/tr/pub/utbd/article/273657>
- [13] Specifications for Buildings to be Built in Seismic Areas (Turkish Earthquake Code), TEC-1975, Ankara, Turkey, 1975.
- [14] Specifications for Buildings to be Built in Seismic Areas (Turkish Earthquake Code), TEC-1998, Ankara, Turkey, 1998.
- [15] Istanbul Seismic Design Code for Tall Buildings, Kandilli Observatory and Earthquake Research Institute, Istanbul, Turkey, 2008.
- [16] *Handbook to the Uniform Building Code: An Illustrative Commentary*, Whittier, CA, USA: International Conference of Building Officials (ICBO), 1994.
- [17] Uniform Building Code, vol. 2, Structural Engineering Design Provisions, Int. Conf. of Building Officials (ICBO), Whittier, CA, USA, 1997.
- [18] Eurocode 8: Design of Structures for Earthquake Resistance, Part 1: General Rules, Seismic Actions and Rules for Buildings, EN 1998-1, European Committee for Standardization (CEN), Brussels, Belgium, 2004.
- [19] NEHRP Recommended Provisions for Seismic Regulations for New Buildings, Part 1: Provisions, FEMA 222A, Federal Emergency Management Agency (FEMA), Washington, DC, USA, 1994.
- [20] NEHRP Recommended Provisions for Seismic Regulations for New Buildings, Part 2: Commentary, FEMA 223A, Federal Emergency Management Agency (FEMA), Washington, DC, USA, 1994.

- [21] NEHRP Recommended Provisions for Seismic Regulations for New Buildings and Other Structures, Part 1: Provisions, FEMA 302, Federal Emergency Management Agency (FEMA), Washington, DC, USA, 1997.
- [22] NEHRP Recommended Provisions for Seismic Regulations for New Buildings and Other Structures, Part 2: Commentary, FEMA 303, Building Seismic Safety Council (BSSC), Washington, DC, USA, 1997.
- [23] Minimum Design Loads for Buildings and Other Structures, ASCE/SEI 7-98, American Society of Civil Engineers (ASCE), Reston, VA, USA, 1998.
- [24] Minimum Design Loads for Buildings and Other Structures, ASCE/SEI 7-02, American Society of Civil Engineers (ASCE), Reston, VA, USA, 2003.
- [25] Minimum Design Loads for Buildings and Other Structures, ASCE/SEI 7-05, American Society of Civil Engineers (ASCE), Reston, VA, USA, 2006.
- [26] Minimum Design Loads for Buildings and Other Structures, ASCE/SEI 7-10, American Society of Civil Engineers (ASCE), Reston, VA, USA, 2010.
- [27] Minimum Design Loads and Associated Criteria for Buildings and Other Structures, ASCE/SEI 7-16, American Society of Civil Engineers (ASCE), Reston, VA, USA, 2017.
- [28] International Building Code, International Code Council (ICC), Falls Church, VA, USA, 2000.
- [29] An Alternative Procedure for Seismic Analysis and Design of Tall Buildings Located in the Los Angeles Region, Los Angeles Tall Buildings Structural Design Council (LATBSDC), Los Angeles, CA, USA, 2008.
- [30] S. Etili and E. M. Güneysi, "Assessment of seismic behavior factor of code-designed steel–concrete composite buildings," *Arab. J. Sci. Eng.*, vol. 46, pp. 4271–4292, May 2021, doi: 10.1007/s13369-020-04913-9. [Online]. Available: <https://doi.org/10.1007/s13369-020-04913-9>
- [31] S. Etili and M. Akgül, "Comparative analysis of composite buildings produced in national and international standards," *Gazi J. Eng. Sci., GJES*, vol. 9, no. 2, pp. 183–199, Aug. 2023. doi: 10.30855/gmbd.0705063. [Online]. Available: <https://doi.org/10.30855/gmbd.0705063>
- [32] S. Etili, "Performance evaluation of steel–concrete composite structures designed in poorly graded soils," *Rev. Constr.*, vol. 22, no. 2, pp. 259–270, Aug. 2023. doi: 10.7764/RDLC.22.2.259. [Online]. Available: <https://doi.org/10.7764/RDLC.22.2.259>
- [33] Computers and Structures, Inc., SAP2000—Integrated Finite Element Analysis and *Design of Structures: Basic Analysis Reference Manual*, Version 14, Berkeley, CA, USA, Aug. 2010.
- [34] N. M. Newmark, "A method of computation for structural dynamics," *J. Eng. Mech. Div.*, vol. 85, no. EM3, pp. 67–94, July 1959.
- [35] Minimum Design Loads and Associated Criteria for Buildings and Other Structures, ASCE/SEI 7-22, American Society of Civil Engineers (ASCE), Reston, VA, USA, 2022.
- [36] Seismic Evaluation and Retrofit of Existing Buildings, ASCE/SEI 41-23, American Society of Civil Engineers (ASCE), Reston, VA, USA, 2023.
- [37] M. S. Beauregard and A. S. Budge, Eds., *Geotechnical Frontiers 2025: Geotechnical Infrastructure*, GSP No. 363. Reston, VA, USA: American Society of Civil Engineers (ASCE), 2025.

- [38] D. T. Cook, A. B. Liel, and A. Safiey, "Earthquake functional recovery in modern reinforced concrete buildings," *J. Struct. Eng.*, vol. 150, no. 9, Jul. 2024. doi: 10.1061/JSENDH.STENG-12904. [Online]. Available: <https://doi.org/10.1061/JSENDH.STENG-12904>
- [39] G. Xu, T. Guo, A.-Q. Li, T. Zhou, and C. Shuang, "Seismic performance of steel frame structures with novel self-centering beams: Shaking-table tests and numerical analysis," *J. Struct. Eng.*, vol. 151, no. 3, Jan. 2025. doi: 10.1061/JSENDH.STENG-13516. [Online]. Available: <https://doi.org/10.1061/JSENDH.STENG-13516>
- [40] Disaster and Emergency Management Authority (AFAD), Turkey Earthquake Hazard Map, Ankara, Türkiye, 2018. [Online]. Available: <https://www.afad.gov.tr>
- [41] Disaster and Emergency Management Authority (AFAD), Turkey Earthquake Hazard Map Update, Ankara, Türkiye, 2023. [Online]. Available: <https://www.afad.gov.tr>
- [42] R. P. Dhakal, "Structural design for earthquake resistance: Past, present and future," in *Structural Engineering and Geomechanics*, vol. II. Oxford, UK: EOLSS Publishers, 2010.
- [43] Federal Emergency Management Agency (FEMA), State-of-the-Art Report on Systems Performance of Steel Moment Frames Subject to Earthquake Ground Shaking, FEMA 355C, Washington, DC, USA, 2000.
- [44] American Institute of Steel Construction (AISC), Specification for Structural Steel Buildings, ANSI/AISC 360-16, Chicago, IL, USA, 2016.
- [45] Pacific Earthquake Engineering Research Center (PEER), PEER Ground Motion Database, University of California, Berkeley, CA, USA, 2018. [Online]. Available: <https://ngawest2.berkeley.edu>
- [46] E. Kalkan and A. K. Chopra, "Practical guidelines to select and scale earthquake records for nonlinear response history analysis of structures," U.S. Geological Survey, Open-File Rep. 2010–1068, Reston, VA, USA, 2010. [Online]. Available: <https://pubs.usgs.gov/of/2010/1068/>
- [47] J. Hancock and J. J. Bommer, "Using spectral matched records to explore the influence of strong-motion duration on inelastic structural response," *Soil Dyn. Earthq. Eng.*, vol. 27, no. 4, pp. 291–299, Apr. 2007, doi: 10.1016/j.soildyn.2006.09.004. [Online]. Available: <https://doi.org/10.1016/j.soildyn.2006.09.004>
- [48] J. Hancock, J. Watson-Lamprey, N. A. Abrahamson, J. J. Bommer, A. Markatis, E. McCoyh, and R. Mendis, "An improved method of matching response spectra of recorded earthquake ground motion using wavelets," *J. Earthq. Eng.*, vol. 10, no. sup001, pp. 67–89, Sep. 2006. doi: 10.1080/13632460609350629. [Online]. Available: <https://doi.org/10.1080/13632460609350629>
- [49] D. N. Grant, "Response spectral matching of two horizontal ground-motion components," *J. Struct. Eng.*, ASCE, vol. 137, no. 3, pp. 289–298, Mar. 2011, doi: 10.1061/(ASCE)ST.1943-541X.0000227. [Online]. Available: [https://doi.org/10.1061/\(ASCE\)ST.1943-541X.0000227](https://doi.org/10.1061/(ASCE)ST.1943-541X.0000227)
- [50] L. Al Atik and N. A. Abrahamson, "An improved method for nonstationary spectral matching," *Earthq. Spectra*, vol. 26, no. 3, pp. 601–617, Aug. 2010. doi: 10.1193/1.3459159. [Online]. Available: <https://doi.org/10.1193/1.3459159>

- [51] NIST, Selecting and Scaling Earthquake Ground Motions for Performing Response-History Analyses, NIST GCR 11-917-15, Gaithersburg, MD, USA, 2011.
- [52] M. Kulak, "Linear time-history analysis of steel structures and the effect of spectrum-matching parameters," M.S. thesis, Dept. of Civil Eng., Eskisehir Technical Univ., Eskisehir, Türkiye, 2019.
- [53] C. Goulet, Y. Bozorgnia, N. Abrahamson, N. Kuehn, L. Al Atik, R. Youngs, and R. Graves, "NGA-East Final Report: Central and Eastern North America Ground-Motion Characterization," PEER Rep. 2018/08, Pacific Earthquake Engineering Research Center, Univ. of California, Berkeley, CA, USA, 2018. [Online]. Available: <https://peer.berkeley.edu/news/new-peer-report-201808-central-and-eastern-north-america-ground-motion-characterization-nga>
- [54] Seismosoft, "SeismoArtif v2023, Release 1: Build 1," Seismosoft Srl, Pavia, Italy, 2023. [Online]. Available: <https://www.seismosoft.com>
- [55] V. Manfredi, A. Masi, A. G. Özcebe, et al., "Selection and spectral matching of recorded ground motions for seismic fragility analyses," *Bull. Earthquake Eng.*, vol. 20, pp. 4961–4987, 2022. doi: 10.1007/s10518-022-01393-0. [Online]. Available: <https://doi.org/10.1007/s10518-022-01393-0>
- [56] A. V. Papageorgiou and C. J. Gantes, "Equivalent uniform damping ratios for linear irregularly damped concrete/steel mixed structures," *Soil Dynamics and Earthquake Engineering*, vol. 31, no. 3, pp. 418–430, Mar. 2011, doi: 10.1016/j.soildyn.2010.09.010. [Online]. Available: <https://doi.org/10.1016/j.soildyn.2010.09.010>